

Ultracold anions for high-precision antihydrogen experiments

G. Cerchiari, P. Yzombard, A. Kellerbauer

Max Planck Institute for Nuclear Physics, Saupfercheckweg 1, 69117 Heidelberg, Germany

M. S. Safronova

Department of Physics and Astronomy, University of Delaware,

217 Sharp Lab, Newark, DE 19716, USA and

Joint Quantum Institute, National Institute of Standards and Technology and
the University of Maryland, Gaithersburg, MD 20742, USA

U. I. Safronova

Physics Department, University of Nevada, Reno, NV 89557, USA

Current and future experiments with antihydrogen ($\bar{\text{H}}$) for a study of matter–antimatter (CPT) symmetry and antimatter gravity require ultracold $\bar{\text{H}}$ in order to reach ultimate levels of precision. A promising path towards the production of anti-atoms much colder than a few kelvin involves the pre-cooling of antiprotons by laser-cooled anions. Due to the unusual binding of the valence electron in anions – dominated by polarization and correlation effects – only few candidate systems with bound–bound transitions suitable for laser cooling exist. We report on a combination of experimental and theoretical studies to fully determine the relevant binding energies, transition rates and branching ratios of the most promising candidate La^- . Using a combination of transverse and collinear laser spectroscopy, we determined the resonant frequency of the laser cooling transition to be $96.592\,713(91)$ THz and the transition rate of its highest-intensity hyperfine component to be $A = 4.90(50) \times 10^4 \text{ s}^{-1}$. We developed a novel relativistic high-precision theoretical treatment of the La^- ion and demonstrate a drastic improvement of theoretical accuracy. Values of yet unmeasured energy levels, transition rates, branching ratios, and level lifetimes calculated in this work complement experimental information on the laser cooling cycle of La^- . The new data establish the suitability of La^- for laser cooling and show that the cooling transition is significantly, by a factor $\approx 50\%$, stronger than previously assumed. Unwanted branching to other decay channels is negligible and can easily be repumped if necessary. Present theoretical methodology may be applied to other negative ions.

INTRODUCTION

Antihydrogen ($\bar{\text{H}}$), the simplest atomic system consisting entirely of antimatter, is an ideal laboratory to search for deviations from the symmetry between matter and antimatter (CPT invariance) and the gravitational acceleration of antimatter (the Weak Equivalence Principle – WEP). Since the first production of cold antihydrogen by the ATHENA collaboration in 2002 [1], several follow-up experiments at CERN’s Antiproton Decelerator (AD) have been conceived in order to study $\bar{\text{H}}$ by laser or microwave spectroscopy (ALPHA [2], ATRAP [3] and ASACUSA [4]) and gravimetry (AEGIS [5, 6] and GBAR [7]), respectively. The production of large amounts of $\bar{\text{H}}$ by several of these experiments, its confinement [8], the observation of the $\bar{\text{H}}$ hyperfine spectrum [9], as well as 1S–2S laser spectroscopy [10], are important milestones towards the physics goals mentioned above.

Presently $\bar{\text{H}}$ is produced at best at the temperature of the cryogenic traps used to confine its constituents, antiprotons (\bar{p}) and positrons (e^+). With the traps cooled by liquid helium, the $\bar{\text{H}}$ temperature is therefore limited to $\approx 4 \dots 10$ K. Trapping in a shallow magnetic trap can further reduce the temperature to ≈ 0.7 K at the expense of a 10^4 reduction in particle number. Several techniques for the production of significantly colder $\bar{\text{H}}$ have been proposed: (1) Direct laser cooling of $\bar{\text{H}}$ with a cw Lyman- α laser [11, 12]; (2) Sympathetic

cooling of $\bar{\text{H}}^+$ with laser-cooled atomic *cations*, followed by photodetachment [13]; and (3) Production of $\bar{\text{H}}$ from \bar{p} sympathetically cooled by laser-cooled *anions* [14, 15].

The latter technique is particularly suited for the AEGIS antimatter gravity experiment, where $\bar{\text{H}}$ will be created by resonant charge exchange between thermal positronium (Ps) and a cloud of \bar{p} confined and pre-cooled in a Penning trap. Due to the large \bar{p} – e^+ mass ratio, the final $\bar{\text{H}}$ temperature will be essentially determined by the initial \bar{p} temperature. This cooling scheme is contingent on the availability of a fast electric-dipole transition in a negative ion. Allowed electronic transitions are rare in atomic anions, where the (weak) binding of the valence electron is dominated by polarization and correlation effects. We initially studied Os^- as a potential laser cooling candidate [16–19], but ultimately had to discard it due to a prohibitively low transition rate of ≈ 50 Hz.

More recently, a new candidate transition was predicted [20] and observed [21] in La^- . The transition connects the $5d^2 6s^2 {}^3\text{F}_2^o$ ground state and the $5d 6s^2 6p {}^3\text{D}_1^o$ excited state. Our measurement of the transition frequency by collinear laser spectroscopy [22] confirmed the initial observation but did not yield a cross-section measurement, and consequently the crucial question of the cooling rate was left unanswered.

In this article we report on a new experiment, which makes use of *transverse* spectroscopy to directly measure the resonant cross-section, as well as new high-precision theoretical

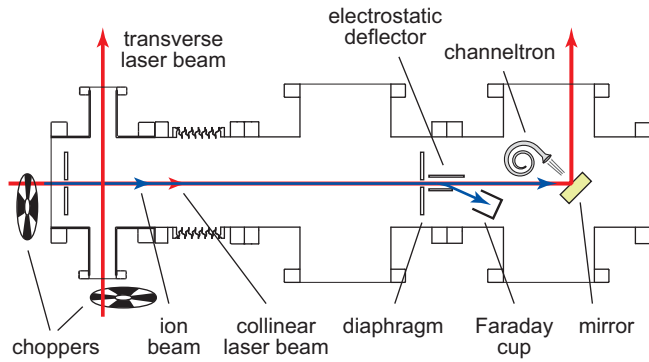


FIG. 1. Sketch of the collinear/transverse laser spectroscopy setup (top view). The ion beam is indicated by a blue line, the laser beams by red lines. The collinear overlap region in this experiment was 730 mm long.

calculations that provide information required for the realization of the laser cooling cycle. Anion laser cooling holds the potential to allow the production of ultracold ensembles of any negatively charged species for other applications as well. As a result, rapid experimental progress in achieving laser cooling with La^- will open a new frontier of ultracold science and enable important applications for tests of fundamental physics.

IMPROVEMENT OF LASER SPECTROSCOPY SETUP

The cross-section of the $^3F_2^e \longleftrightarrow ^3D_1^o$ transition was measured with a setup similar to the one described in Ref. [22], but improved in several important aspects. The main difference is the introduction of new laser viewports to allow transverse excitation of the continuous ion beam, a prerequisite for a precise cross-section measurement.

Briefly, ions are produced and accelerated to 7 keV from a Cs sputter source. The beam of La^- is selected by a 90° dipole bending magnet and, further downstream, electrostatically deflected by another 90° into a field-free drift region. Along the straight section the beam is collimated by two circular apertures with radius $r = 3.25$ mm placed a distance $d = 730$ mm apart. After the last aperture two parallel-plate electrodes deflect ions into a Faraday cup for current monitoring. Neutral particles present in the beam pass straight ahead, through another 4 mm radius aperture. Transmitted neutral atoms are counted by a channeltron detector via secondary-electron emission from the surface of a gold mirror.

In the new setup shown in Fig. 1, the mirror is inclined by 45° with respect to the incoming beam direction and placed at a potential of -500 V with respect to the entrance of the channeltron to favor electron detection. Four 25.4 mm windows allow introducing light into the straight section. Two windows are used to couple light collinearly with the ion beam path, exploiting the reflection on the gold mirror. The second pair of windows allows orthogonal access 60 mm downstream of the first collimating aperture.

The laser light used in this experiment is produced by a cw optical parametric oscillator (OPO) system (Aculight Argos Model 2400) able to generate ≈ 1.5 W of light near the wavelength of interest with a nominal linewidth < 1 MHz. The laser is superimposed collinearly and transversely onto the ion beam with a 30:70 intensity ratio, respectively. The laser power profile was measured to have a radial Gaussian shape $W(R) \propto \exp(-2R^2/w^2)$, where R is the radial dimension. The width was measured to be $w = 2.69(5)$ mm for the transverse beam after a twofold reduction by a telescope lens system. The intensity illuminating ions in the transverse direction is set by a half-wave plate combined with a polarizer. The collinear beam is modified neither in shape nor in intensity. It is, however, reflected once along its path. Due to incomplete overlap of the reflected beam as well as the laser's natural divergence, uniform collinear irradiance of the ion beam was assumed.

In all experiments, the laser frequency was set to (or scanned around) the transition from the $^3F_2^e$ ground to the $^3D_1^o$ excited state. Because the binding energy of the excited state is ≈ 160 meV, the absorption of a second photon of energy ≈ 400 meV leads to photodetachment. Due to the much larger interaction volume, the detachment step is much (≈ 30 times) more likely to be caused by the collinear beam. At the same time, the collinear beam is out of resonance with the transition due to the Doppler effect. Consequently, for the purpose of this measurement, independence of the two excitation steps was assumed. When the transverse laser frequency matches the transition frequency, an increased neutral count rate is registered. Both laser components are chopped, at 25 Hz (transverse) and 5 Hz (collinear), and the integrated neutral counts are recorded every 2 s. Each data point hence consists of four values corresponding to the possible chopper states. The output signal is obtained by subtracting the counts with either laser illuminating the ions from those with both lasers on. In order to correctly take into account the background, the counts acquired with both lasers off must once again be added.

As is the case for the collinear laser beam, the transverse beam can also be reflected back through the ion beam. Assuming sufficient laser intensity, this can be used to carry out Doppler-free saturation spectroscopy. A shutter with a 4 s period obstructs the reflected beam, such that the signals corresponding both to single and to double transverse illumination can be recorded.

CROSS-SECTION MEASUREMENT

A prerequisite for the cross-section measurement was the confirmation of the rest frame transition frequency of our previous work [22]. For this purpose, the alignment of the primary and reflected transverse laser beams was optimized by comparing the single- and double-pass data. This eliminates any frequency shift associated with a non-perpendicular alignment of the ion and laser beams and allows a reduction of the observed linewidth by saturation spectroscopy. With single-

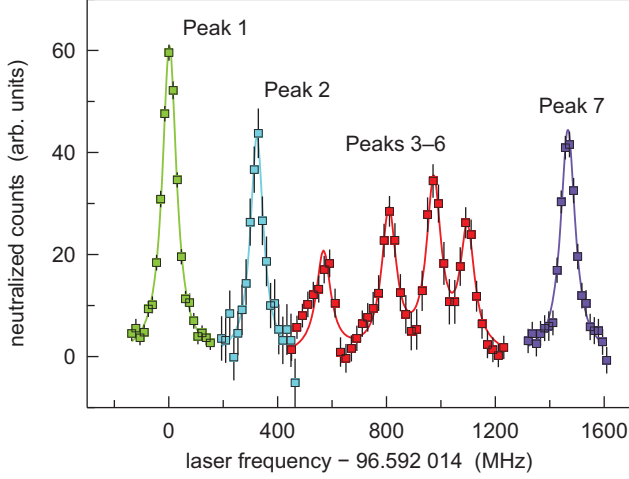


FIG. 2. Composite graph of the ${}^3F_2^e \rightarrow {}^3D_1^o$ resonance in La^- , resolving its hyperfine structure. Different colors correspond to four different acquisitions combined in this plot. Solid lines are Lorentzian fits of the peaks. The FWHM of Peaks 1–6 was found to be 64.3(1.5) MHz.

TABLE I. Hyperfine transition frequencies with respect to $11/2 \leftrightarrow 9/2$ [at an absolute frequency of 96.592 014(05)(75) THz]. Transitions are listed by total angular momentum F of the ground (left) and excited states (right).

Peak no.	Hyperfine transition	Transition frequency (MHz)	
		Exp. [22]	this work
1	$11/2 \leftrightarrow 9/2$	0.0(5.8)	0.0(3.5)
2	$9/2 \leftrightarrow 7/2$	324.8(5.8)	321.6(4.6)
3	$7/2 \leftrightarrow 5/2$	604.1(5.9)	585.8(5.8)
4	$9/2 \leftrightarrow 9/2$	825.1(5.8)	814.2(5.2)
5	$7/2 \leftrightarrow 7/2$	990.1(5.9)	977.2(5.2)
6	$5/2 \leftrightarrow 5/2$	1116.2(6.1)	1102.5(5.2)
7a	$3/2 \leftrightarrow 5/2$	1480.2(5.8)	1467.6(4.0)
7b	$5/2 \leftrightarrow 7/2$		
7c	$7/2 \leftrightarrow 9/2$		

pass transverse spectroscopy, the width of individual hyperfine peaks reached $\Gamma_{\text{res}} > 150$ MHz (FWHM of the Gaussian resonance) in the presence of power broadening. In double-pass configuration, the width was reduced to < 65 MHz (FWHM of the Lorentzian resonance) in the Doppler-free spectrum. This latter value is limited by the interaction time of the ions with the transverse laser (time-of-flight broadening), but improves our previous result of $\Gamma_{\text{res}} \approx 75$ MHz obtained by collinear spectroscopy.

Figure 2 shows the entire hyperfine spectrum of the ${}^3F_2^e \rightarrow {}^3D_1^o$ transition, assembled from separate measurements of individual hyperfine transitions or groups thereof. The measured frequencies of the hyperfine transitions (see Tab. I) agree well with our previous values obtained by collinear spectroscopy [22]. As in the prior work, the internal structure

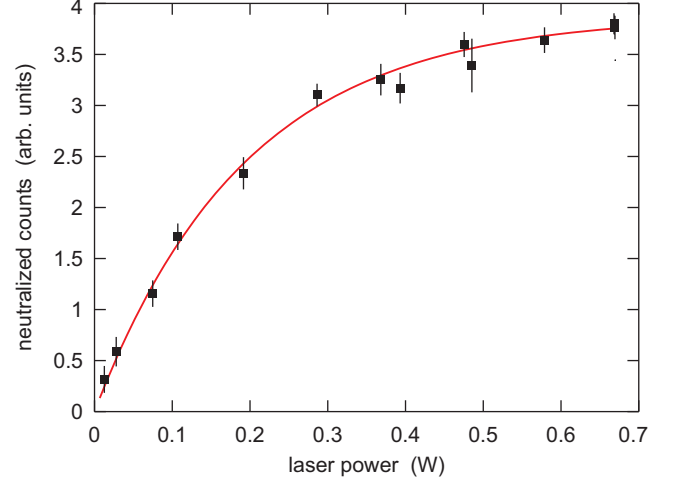


FIG. 3. Neutral atoms detected as a function of transverse laser beam power. The solid red line is a fit with the function of Eq. (2).

of the highest-frequency peak (consisting of three hyperfine transitions) was not resolved. The center-of-gravity frequency was found to be 96.592 713(52)(75) THz, where the first number in parentheses represents the statistical uncertainty and the second the systematic uncertainty, in good agreement with our prior result of 96.592 80(10) THz.

The resonant cross section σ was measured using the hyperfine transition with angular momentum quantum numbers $F = 11/2 \leftrightarrow 9/2$ (Peak 1). In this measurement, the laser reflection used to obtain the Doppler-free spectrum was blocked. The relative change of detected neutral La atoms N was monitored as a function of the laser power W_0 , with the frequency fixed on resonance. A typical graph of this dependency is shown in Fig. 3. The relation linking those quantities was obtained by analytically solving the associated rate equations, see Methods. Several $N(W_0)$ graphs were recorded for slightly different spatial overlap between the ion and transverse laser beams. For this purpose, the vertical incident angle of the laser was varied.

Care was also taken to ensure that possible fluctuations in ion current could not affect the measurement. For this purpose, the dependence $n(W_0)$ was recorded by scanning the curve from high to low power and back while ensuring the consistency of data acquired at the beginning and at the end of the measurement sequence. Finally, an observed cross-section of $\sigma = 1.0(1) \times 10^{-12} \text{ cm}^2$ was obtained by interpolating the data to the maximal overlap. With an experimental transition width $\Gamma_{\text{res}} = 119.6(2.5)$ MHz (without power broadening), we find an excited-state lifetime of $\tau_{\text{exp}} = c^2/(4\pi^2\sigma\nu^2\Gamma_{\text{res}}) = 20.4(2.1) \mu\text{s}$. This value retrospectively justifies the approximation of neglecting spontaneous emission in the rate equations, since decay is very improbable during the short time in which ions travel through the transverse laser that drives the first excitation step.

TREATMENT OF CORRELATIONS IN CALCULATING ANION PROPERTIES

Accurate theoretical predictions of La^- properties, in particular the positions of yet unmeasured energy levels, transition rates and branching ratios, are crucial for the development of experimental laser cooling schemes and for evaluating their performance. Calculating anion properties is a very difficult task, with the complicated electronic structure of lanthanides presenting major difficulties due to the large electronic correlations. While the best calculation of the La^- bound spectra to date, carried out by the relativistic configuration interaction (RCI) method [23], provided guidance in identifying the measured lines of La^- spectra [21], the differences between the theoretical predictions and the measured excitation energies are as high as 17...33%.

The guiding principle of our approach is to treat La^- as an atomic system with a Xe-like core with 54 electrons and four additional valence electrons. In this way, the treatment of the electronic correlations separates into two problems: (1) Strong valence–valence correlations and (2) Inclusion of core–valence correlations for such a large core. The main reason for the discrepancy of the previous theory [23] with experiment is the omission of the latter contribution in the framework of the RCI approach. In the present work we use a hybrid approach that efficiently treats these two correlations by separate methods [24].

The first problem is treated by a very-large-scale CI method in the four-electron valence space. The many-electron wave function is obtained as a linear combination of all distinct four-electron states Φ_i of a given angular momentum J and parity:

$$\Psi_J = \sum_i c_i \Phi_i. \quad (1)$$

In the usual implementation of the CI, the energies and wave functions of the low-lying states are determined by diagonalizing the Hamiltonian: $H = H_1 + H_2$, where H_1 is the one-body part of the Hamiltonian and H_2 the two-body part, which contains Coulomb and Breit matrix elements. In our method, this bare Hamiltonian is replaced by the effective one,

$$\begin{aligned} H_1^{\text{eff}} &\rightarrow H_1 + \Sigma_1 \\ H_2^{\text{eff}} &\rightarrow H_2 + \Sigma_2, \end{aligned}$$

where the Σ_i corrections incorporate all single and double excitations from *all* core shells to all basis set orbitals, efficiently solving the second problem. In this way, the properties of a lanthanide anion can be calculated to high-precision for the first time: the accuracy of our theoretical energies is 0.2...2%. Moreover, our method allows estimating the uncertainties in yet unmeasured values of other energy levels and transition properties.

Such an effective Hamiltonian H^{eff} can be constructed either using second-order perturbation theory (CI+MBPT method, [25, 26]) or the more accurate all-order coupled-cluster method (CI+all-order method, [24]). The CI method

is then applied as usual with the modified H^{eff} to obtain improved energies and wavefunctions. Matrix elements and other properties, such as electric-multipole and magnetic-dipole transition matrix elements, can be determined using the resulting wavefunctions.

The CI+all-order method has been applied to neutral atoms and ions with few valence electrons [27–29]. However, it has never been considered for negative ions, as it was generally assumed that such computations for weakly bound states of negative ions would be numerically unstable. The electron in an anion is extremely weakly bound since the nucleus is effectively screened by the electron cloud. This leads to a poor convergence of the valence CI as additional configurations are included. We find that this is indeed the case for smaller sets of CI configurations, yielding unexpected spurious low-lying configurations in La^- bound spectra.

The number of configurations Φ_i that have to be considered grows exponentially with the number of valence electrons. To resolve this problem, we developed an algorithm to efficiently select dominant configurations and performed extensive tests of our method for La^- . To ensure the completeness of the CI space, we carried out five large-scale CI+all-order calculations with an increasing size of the four-electron configuration space to ensure that it was sufficiently large. We also performed CI+MBPT calculations to evaluate the importance of the higher-order corrections to the effective Hamiltonian and evaluate the uncertainties of the results.

ELECTRON AFFINITY AND BOUND ENERGY LEVELS

The electron affinity $EA(X)$ of an atom X is defined as the difference between the total energy of the ground state of X and that of its negative ion X^- [30]. It is positive for stable negative ions. The calculation of electron affinities is very sensitive to the details of the computations of the neutral and negative ion energies. In our method, CI+all-order calculations for La and La^- share the same effective Hamiltonian constructed in the Dirac–Fock potential of the same Xe core. Therefore, they share the same core energy, and the affinity is calculated as the difference of the ground-state valence energies of La and La^- . Our affinity value $EA(X) = 560(14)$ meV disagrees with the experimental result of 470(20) meV [31], so we carried out a detailed evaluation of the accuracy of our value, as described in Methods. We note that both the theoretical work of Ref. [23] and the experimental results of Ref. [21] indicate a larger affinity, consistent with our prediction.

Our CI+all-order results on bound energy levels are compared with the experimental values of Ref. [21] and the theoretical results of Ref. [23] in Tab. II. Our values are in excellent agreement with experimental data. We predict a number of yet unmeasured La^- bound states, in particular the $6s^2 5d^2 \ ^3P_J$ triplet. Our calculations show that the even $6s^2 5d^2 \ ^3P_0$ level is much closer to the upper cooling transition level $6s^2 5d 6p \ ^3D_1$ than indicated by Ref. [23]. The energy difference is on the order of our computational accuracy.

TABLE II. Level energies in La^- evaluated using the CI+all-order method, relative to the $6s^2 5d^2 \ ^3F_2$ ground state. The last column gives the difference with experiment (in %).

Config.		Level energy (meV)			
		Theo. [23]	Exp. [21]	this work	Diff.
$6s^2 5d^2$	3F_3	67	83.94	83.75	+0.2%
	3F_4	135	172.9	174.8	-1.1%
	1D_2	286		328.1	
	3P_0	417		410.2	
	3P_1	442		440.4	
	3P_2	493		504.7	
$6s^2 5d6p$	1D_2	111		217.9	
	3F_2	259	343.7	345.8	-0.6%
	3F_3	305	383.9	389.1	-1.4%
	3D_1	337	399.4	406.9	-1.9%
	3D_2	396	470.6	478.5	-1.7%
	3F_4	406	496.2	502.9	-1.4%
	3P_0	535		548.6	
	3D_3	461	538.8	549.3	-2.0%

However, we find that the position of the $^3P_0^e$ level is largely unaffected by the number of configurations included in the valence CI. It varies by less than 1 meV for two large-scale calculations, while the $^3D_1^o$ level shifts by as much as 10 meV, indicating a higher accuracy of the prediction for even levels.

The E1 matrix element for the transition between the $^3P_0^e$ level and the $^3D_1^o$ level is $1.17 \ e a_0$, where a_0 is the Bohr radius. If the metastable 3P_0 level is energetically lower, it will be populated with a small probability. The branching ratio would strongly depend on the transition energy. We estimate the branching ratio to be very small, $3 \times 10^{-7} \dots 1 \times 10^{-6}$ (for a separation energy $3 \dots 5$ meV between these two levels.) It would be useful to measure the excitation energy of any of the 3P_J levels to benchmark our theoretical predictions.

TRANSITION RATES, BRANCHING RATIOS AND LIFETIMES

We calculated the electric-dipole matrix elements for allowed La^- transitions using both CI+MBPT and three variants of CI+all-order wavefunctions with increasing numbers of configurations. The transition rates, branching ratios and lifetimes relevant for the laser cooling cycle are given in Tab. III. We used experimental energies from Ref. [21], where available, in the transition rate, branching ratio and lifetime calculations. All calculations include random-phase-approximation corrections to the electric-dipole operator. The uncertainties of the final values were estimated by performing several different computations. The difference of the CI+all-order and CI+MBPT results gives an estimate of the higher-order correlation corrections, and we took this as an estimate of omitted higher-order corrections. The uncertainty associ-

TABLE III. Transition rates A_r (in s^{-1}), branching ratios, and lifetimes τ of transitions in La^- calculated using the CI+all method. Experimental energies from Ref. [21] were used in the transition rate, branching ratio and lifetime calculations, where available. Numbers in brackets represent powers of 10.

Upper level	Lower level	A_r (s^{-1})	Branching ratio	τ
$6s^2 5d6p \ ^3D_1$	$6s^2 5d^2 \ ^3F_2$	4.54[+4]	0.999974	22.1 μs
	$6s^2 5d^2 \ ^1D_2$	1.18[0]	0.000026	
$6s^2 5d^2 \ ^1D_2$	$6s^2 5d6p \ ^1D_2$	1.95[0]	0.956	489 ms
	$6s^2 5d^2 \ ^3F_2$	9.00[-2]	0.044	
$6s^2 5d6p \ ^1D_2$	$6s^2 5d^2 \ ^3F_2$	1.68[+2]	0.791	4.71 ms
	$6s^2 5d^2 \ ^3F_3$	4.44[+1]	0.209	
$6s^2 5d^2 \ ^3F_3$	$6s^2 5d^2 \ ^3F_2$	7.56[-3]	1.0	132 s
$6s^2 5d6p \ ^3D_2$	$6s^2 5d^2 \ ^3F_2$	4.50[+3]	0.1059	23.5 μs
	$6s^2 5d^2 \ ^3F_3$	3.79[+4]	0.8924	
	$6s^2 5d^2 \ ^1D_2$	4.41[+1]	0.0010	
	$6s^2 5d^2 \ ^3P_1$	2.75[+1]	0.0006	

ated with the CI space completeness was estimated as the difference of the matrix elements obtained with two large-scale computations with increasing number of configurations.

We combined these two uncertainties – carefully accounting for the cases where they cancel – to provide an estimate of the matrix element uncertainties. These are rough estimates and likely to be overestimated. For example, our energy levels are in much better agreement with experiment than the difference of the CI+MBPT and CI+all-order values. In general, weak matrix elements are more poorly calculated due to the much larger relative size of the correlation corrections and stronger effects of configuration mixing. Nevertheless, our estimates give some guidance on the accuracy of the transition rates, distinguishing the cases where 2...5% uncertainties are expected from those where 25% uncertainties are expected. In the cases where transition energies are experimentally known, the relative uncertainties of the transitions rates are twice those of the matrix elements. Ultimately, we estimate the uncertainty of the transition rate of the $5d6p \ ^3D_1 \rightarrow 5d^2 \ ^3F_2$ laser cooling transition to be 4%. The corresponding theoretical lifetime value $\tau_{\text{theo}} = 22.1(9) \ \mu\text{s}$ can be directly compared to the experimental result $\tau_{\text{exp}} = 20.4(2.1) \ \mu\text{s}$ because in the absence of other dipole-allowed transitions from the 11/2 hyperfine level of the ground state, the measured rate of the $11/2 \rightarrow 9/2$ transition is equal to the total decay rate from the excited state. Taking into account the respective uncertainties, our experimental and theoretical values are in excellent agreement.

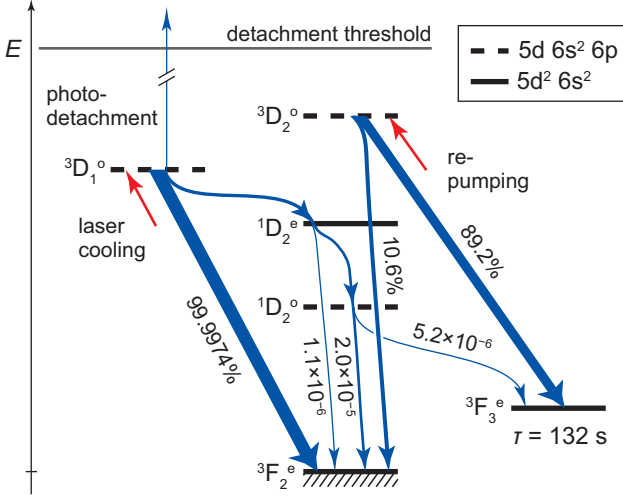


FIG. 4. Partial energy level diagram of La^- (energies to scale). The relevant decay branches from the $^3\text{D}_1^\circ$ excited state of the laser cooling transition, as well as from the $^3\text{D}_2^\circ$ excited state of the repumping transition are indicated. Thicknesses of blue arrows are indicative of branching ratios, but not to scale.

DISCUSSION

The determined transition rates and branching ratios are crucial for the implementation of the cooling cycle. Our present value for the rate of the laser cooling transition (averaged over all hyperfine components) is $A_r \approx 4.5 \times 10^4 \text{ s}^{-1}$, about 50% larger than the previous prediction $2.9 \times 10^4 \text{ s}^{-1}$ [20]. The laser-cooled ensemble will thus reach the Doppler temperature T_D (or the equilibrium temperature in case of competing heating processes) faster than previously assumed. For instance, a simple calculation shows that 1-dimensional cooling of an ensemble of La^- ions confined in a Paul trap from 100 K to T_D will require the absorption of 8.4×10^4 photons, and hence take 3.7 s in saturation.

Another important factor in considering a laser cooling transition is the degree to which the cooling cycle is closed. We can fully deduce all relevant branchings from our present results, as illustrated in the partial energy level diagram of Fig. 4. Branchings at least two orders of magnitude smaller than those indicated have been neglected. The excited $^3\text{D}_1^\circ$ state will decay to the $^3\text{F}_2^\circ$ ground state in all but 2.6×10^{-5} of cases. However, only a total 5.2×10^{-6} branching to the $^3\text{F}_3^\circ$ state is potentially problematic, because that state cannot decay to the ground state by an electric-dipole transition and is hence metastable (lifetime $\tau = 132 \text{ s}$). Thus, after scattering 8.4×10^4 photons, roughly 40% of all anions end up in the metastable state. If necessary, the $^3\text{F}_3^\circ \rightarrow ^3\text{D}_2^\circ$ transition can be repumped, as shown in the figure.

Finally, photodetachment from the $^3\text{D}_1^\circ$ excited state may remove La^- ions from the trap before laser cooling is complete. The cross-section of the (non-resonant) photodetachment process is about five orders of magnitude smaller than

that of the resonant laser excitation. In addition to its cross-section, the photodetachment rate also depends on the fraction of time during which ions populate excited states, and hence on the saturation. Assuming the power of the cooling laser is chosen such that the saturation parameter is $s = 2$, the photodetachment rate is 0.024 s^{-1} and the branching to photodetachment is 5.3×10^{-7} . Hence, again assuming 8.4×10^4 cooling cycles, a fraction of about 10% of La^- ions would be lost by the time the remaining ensemble has reached the Doppler temperature.

ACKNOWLEDGMENTS

We thank the MPIK accelerator group and workshop for invaluable assistance with the ion source. We thank Sergey Porsev and Mikhail Kozlov for helpful discussions. The experimental work was supported by the European Research Council (ERC) under Grant No. 259209 (UNIC). The theoretical work was performed under the sponsorship of the U.S. Department of Commerce, National Institute of Standards and Technology.

METHODS

Rate equations and geometrical overlap

The rate equations were simplified to a two-level system describing the bound-bound transition while assuming the independence of the two excitation steps and neglecting spontaneous decay from the excited state. The expression for the number of neutral La atoms N is also a function of the velocity v of the ions, the laser frequency ν and a geometrical factor g , which depends on the overlap of the ion-laser beam:

$$N(W_0) \propto 1 - \exp\left(-\sigma \frac{W_0}{h\nu} \frac{1}{v} g\right). \quad (2)$$

To simplify the geometry the reflected transverse beam was blocked. For perfectly overlapping axes of the ion and laser beams and uniform ion beam density the geometrical factor is

$$g = \frac{1}{w} \sqrt{\frac{8}{\pi}} \exp\left(-\frac{r^2}{w^2}\right) \left(I_0\left(\frac{r^2}{w^2}\right) + I_1\left(\frac{r^2}{w^2}\right) \right),$$

where I_n is a modified Bessel function of the first kind.

Uncertainty in the theory affinity value

There are three main sources of uncertainty in the affinity value in our calculations: (1) The uncertainty associated with the saturation of the CI space of the La calculation: We estimate this to be 5 meV, calculated as the difference of two La calculations with an extra 5000 configurations, selected from the dominant set; (2) The uncertainty associated with

the saturation of the CI space of the La^- calculation: We estimate this to be 9 meV, calculated as the difference of two large-scale calculations with increased number of configurations; (3) The uncertainty associated with the treatment of the higher-order core–valence correlations: We estimate this to be 9 meV, calculated as the difference of CI+MBPT and CI+all-order calculations for La^- . Adding these three uncertainties in quadrature yields the final value of 14 meV.

Calculation of transition rates and lifetimes

The multipole transition rates A_{ab} are determined using the formulas:

$$A(E1) = \frac{2.02613 \times 10^{18}}{(2J_a + 1)\lambda^3} S(E1), \quad (3)$$

$$A(M1) = \frac{2.69735 \times 10^{13}}{(2J_a + 1)\lambda^3} S(M1), \quad (4)$$

$$A(E2) = \frac{1.11995 \times 10^{18}}{(2J_a + 1)\lambda^5} S(E2), \quad (5)$$

where the wavelength λ is in Å and the line strength S is in atomic units. The line strengths S are determined as the squares of the corresponding reduced matrix elements. The lifetime of a state a is calculated as

$$\tau_a = \frac{1}{\sum_b A_{ab}}.$$

-
- [1] M. Amoretti *et al.* (ATHENA Collaboration), *Nature* **419**, 456 (2002).
 - [2] C. L. Cesar *et al.* (ALPHA Collaboration), *Can. J. Phys.* **87**, 791 (2009).
 - [3] G. Gabrielse, P. Laroche, D. Le Sage, B. Levitt, W. S. Kolthammer, R. McConnell, P. Richerme, J. Wrubel, A. Speck, M. C. George, D. Grzonka, W. Oelert, T. Sefzick, Z. Zhang, A. Carew, D. Comeau, E. A. Hessels, C. H. Storry, M. Weel, and J. Walz (ATRAP Collaboration), *Phys. Rev. Lett.* **100**, 113001 (2008).
 - [4] N. Kuroda *et al.* (ASACUSA Collaboration), *Nature Commun.* **5**, 3089 (2014).
 - [5] A. Kellerbauer *et al.* (AEGIS Proto-Collaboration), *Nuclear Instrum. Methods B* **266**, 351 (2008).
 - [6] M. Doser *et al.* (AEGIS Collaboration), *Class. Quantum Grav.* **29**, 184009 (2012).
 - [7] P. Indelicato *et al.* (GBAR Collaboration), *Hyp. Int.* **228**, 141 (2014).
 - [8] G. B. Andresen *et al.* (ALPHA Collaboration), *Nature* **468**, 673 (2010).
 - [9] M. Ahmadi *et al.* (ALPHA Collaboration), *Nature* **548**, 66 (2017).
 - [10] M. Ahmadi *et al.* (ALPHA Collaboration), *Nature* **541**, 506 (2017).
 - [11] S. Wu, R. C. Brown, W. D. Phillips, and J. V. Porto, *Phys. Rev. Lett.* **106**, 213001 (2011).
 - [12] P. H. Donnan, M. C. Fujiwara, and F. Robicheaux, *J. Phys. B* **46**, 025302 (2013).
 - [13] L. Hilico, J.-P. Karr, A. Douillet, P. Indelicato, S. Wolf, and F. Schmidt Kaler, *Int. J. Mod. Phys. Conf. Series* **30**, 1460269 (2014).
 - [14] A. Kellerbauer and J. Walz, *New Journal of Physics* **8**, 45 (2006).
 - [15] P. Yzombard, M. Hamamda, S. Gerber, M. Doser, and D. Comparat, *Phys. Rev. Lett.* **114**, 213001 (2015).
 - [16] U. Warring, M. Amoretti, C. Canali, A. Fischer, R. Heyne, J. O. Meier, C. Morhard, and A. Kellerbauer, *Phys. Rev. Lett.* **102**, 043001 (2009).
 - [17] A. Fischer, C. Canali, U. Warring, A. Kellerbauer, and S. Fritzsche, *Phys. Rev. Lett.* **104**, 073004 (2010).
 - [18] A. Kellerbauer, C. Canali, A. Fischer, U. Warring, and S. Fritzsche, *Phys. Rev. A* **84**, 062510 (2011).
 - [19] A. Kellerbauer, A. Fischer, and U. Warring, *Phys. Rev. A* **89**, 043430 (2014).
 - [20] S. M. O'Malley and D. R. Beck, *Phys. Rev. A* **81**, 032503 (2010).
 - [21] C. W. Walter, N. D. Gibson, D. J. Matyas, C. Crocker, K. A. Dungan, B. R. Matola, and J. Rohln, *Phys. Rev. Lett.* **113**, 063001 (2014).
 - [22] E. Jordan, G. Cerchiari, S. Fritzsche, and A. Kellerbauer, *Phys. Rev. Lett.* **115**, 113001 (2015).
 - [23] S. M. O'Malley and D. R. Beck, *Phys. Rev. A* **79**, 012511 (2009).
 - [24] M. S. Safronova, M. G. Kozlov, W. R. Johnson, and D. Jiang, *Phys. Rev. A* **80**, 012516 (2009), arXiv:0905.2578 [physics.atom-ph].
 - [25] V. A. Dzuba, V. V. Flambaum, and M. G. Kozlov, *Phys. Rev. A* **54**, 3948 (1996).
 - [26] M. G. Kozlov, S. G. Porsev, M. S. Safronova, and I. I. Tupitsyn, *Computer Physics Communications* **195**, 199 (2015).
 - [27] M. S. Safronova, U. I. Safronova, and C. W. Clark, *Phys. Rev. A* **90**, 032512 (2014), arXiv:1408.3067 [physics.atom-ph].
 - [28] M. S. Safronova, U. I. Safronova, and C. W. Clark, *Phys. Rev. A* **91**, 022504 (2015).
 - [29] S. G. Porsev, M. G. Kozlov, M. S. Safronova, and I. I. Tupitsyn, *Phys. Rev. A* **93**, 012501 (2016), arXiv:1510.06679 [physics.atom-ph].
 - [30] T. Andersen, H. K. Haugen, and H. Hotop, *J. Phys. Chem. Ref. Data* **28**, 1511 (1999).
 - [31] A. M. Covington, D. Calabrese, J. S. Thompson, and T. J. Kvale, *J. Phys. B* **31**, L855 (1998).